Journal of Physics: Condensed Matter

PAPER

On the mechanisms of tip-force induced switching in ferroelectric thin films: the crossover of depolarization, shear strain and flexoelectricity

To cite this article: L L Ma *et al* 2019 *J. Phys.: Condens. Matter* **31** 145701

IOP Publishing Journal of Physics: Condensed Matter

J. Phys.: Condens. Matter **31** (2019) 145701 (18pp) https://doi.org/10.1088/1361-648X/aafdf2

On the mechanisms of tip-force induced switching in ferroelectric thin films: the crossover of depolarization, shear strain and flexoelectricity

L L Ma[1,2,3], W J Chen[1,2,4], Y L Liu[3], Biao Wang[1,5] and Yue Zheng[1,2]

[1] State Key Laboratory of Optoelectronic Materials and Technologies, School of Physics, Sun Yat-sen University, 510275 Guangzhou, People's Republic of China
[2] Micro and Nano Physics and Mechanics Research Laboratory, School of Physics, Sun Yat-sen University, 510275 Guangzhou, People's Republic of China
[3] School of Engineering, Sun Yat-sen University, 510275 Guangzhou, People's Republic of China
[4] School of Materials, Sun Yat-sen University, 510275 Guangzhou, People's Republic of China
[5] Sino-French Institute of Nuclear Engineering and Technology, Sun Yat-sen University, 519082 Zhuhai, People's Republic of China

E-mail: zhengy35@mail.sysu.edu.cn, chenweijin@mail.sysu.edu.cn and wangbiao@mail.sysu.edu.cn

Received 13 November 2018, revised 6 January 2019
Accepted for publication 11 January 2019
Published 13 February 2019

Abstract

The recent observation of mechanical switching of ferroelectric polarization has placed the mechanical manipulation of ferroelectrics on an equal footing with the conventional electrical manipulation. However, discussions on the exact switching mechanisms due to mechanical loads are ongoing for the complexity in experimental situations. In this work, based on continuum mechanical and thermodynamic modeling and simulation, we analyze the mechanisms of tip-force induced switching in ferroelectric thin films. The roles of depolarization, shear strain and flexoelectricity in mechanical switching, both in normal and sliding loading modes, are separated out and the switching characteristics are analyzed. The depolarization field in the film is demonstrated to enable bidirectional switching. The coupling between shear strain and polarization components is shown to be important in the sliding loading mode. A great influence of flexoelectricity-modified polarization boundary condition on the switching process is revealed. The previous speculation that the switching process experiences an intermediate paraelectric phase is proved. The regulation of loading force, misfit strain, temperature and film thickness on the switching are further given for each mechanism. Taking all of the three mechanisms into account, we present the phase diagrams of mechanical switching for films in an initial upward or downward polarization state. The revealed characteristics of various switching mechanisms should provide useful guidelines for their verification in experiments, and the tunability of the switching by various influencing factors is instructive for the design and optimization of ferroelectric devices via mechanical engineering.

Keywords: ferroelectrics, mechanical switching, depolarization, shear strain, flexoelectricity

S Supplementary material for this article is available online

(Some figures may appear in colour only in the online journal)

1. Introduction

Ferroelectric nanofilms have raised enormous attention in the past two decades for outstanding functional properties such as ferroelectricity, dielectricity, piezoelectricity [1, 2], photovoltaic effect [3], polarization-related conductivity [4], etc, and present promising prospect in development of sensors, actuators, transducers, and non-volatile memories [5–7]. The ferroelectric domain patterns in the film can impose significant influences on material properties, therefore domain engineering has been proved as an efficient way to tune the functionalities of the film [8, 9]. Electric field has been demonstrated an effective load to control the ferroelectric domains. However, electrical manipulation also suffers from some well-known problems such as the occurring of charge injection, leakage current and electrical breakdown, leading to degradation and failure of the ferroelectric devices. Mechanical approaches, such as substrate strain engineering, which bring us alternative ways to obtain desirable domain patterns without the use of external electric field, have shown great application potentials in the MEMS devices [10–12].

A recent focusing issue in ferroelectrics is the mechanical switching of ferroelectric polarization, which has injected new vitality in the field of ferroelectrics as it places the issue of mechanical manipulation of ferroelectrics on an equal footing with the common electrical manipulation. The typical work by Lu *et al* demonstrated the switchability of ferroelectric polarization via the force of a piezoelectric force microscopy (PFM) tip, where the initial upward polarization of $BaTiO_3$ (BTO) nanofilm was switched into a downward state by pressing the PFM tip onto the film surface [13]. Since then, lots of investigations have been focused on this mechanical writing phenomenon of ferroelectric polarization. In the experimental aspect, polarization switching under tip loads has been discovered not only in ferroelectric ceramics, but also in polymers [11]. The misfit strain has been demonstrated to have significant effect on the critical switching force, showing that a smaller compressive strain is favored to switch the polarization of the nanofilm [14, 15]. The loading mode of the PFM tip force was also found to have impacts on the mechanical switching behaviors. It was shown that the sliding mode where friction force is involved could result in bigger and more stable switched domains than the normal loading mode [16]. More recently, it was also reported that the multiaxial bismuth ferrite (BFO) could present multiple domain switching pathways under sliding PFM tip forces [17]. Selective control of these pathways could be realized by choosing proper sliding directions. On the other hand, theoretical studies are focused on understanding the mechanisms of mechanical switching and revealing the switching characteristics. The driving force of the mechanical switching was at first naturally attributed to the flexoelectric effect [13], i.e. the coupling between polarization and strain gradient [18, 19]. In this regime, the large strain gradient in the vicinity of tip-film contact area under the tip loads induces the so-called flexoelectric field, which can exceed the coercive field of the polarization and result in the polarization switching. Phase field simulations have been conducted to validate this mechanism [20, 21]. Besides, the ionized defects such as the oxygen vacancies in the film, will be compelled and redistribute under the tip force and then change the internal electric field of the film. Such an effect has been shown to be capable of inducing mechanical switching in films thicker than 20 nm [22]. Another possible source of polarization switching is the incomplete screening condition due to the surface charge electrochemistry, which can result in a large depolarization field under the tip force and give rise to mechanical switching [22–25]. Specially, the surface screening effect was predicted to enable interesting mechanical switching behaviors, e.g. bidirectional switching and propagating switching modes [25]. In addition, it was reported that the coupling between shear strain and polarization could be also exploited to induce mechanical switching when the ferroelectric film adopts an orthorhombic or rhombohedral phase [26].

Despite these abundant investigations devoted to the issue of mechanical switching, discussions on the exact switching mechanisms are still ongoing due to the complexity in real situations. On the one hand, it is a fundamental question to ask: does there exist any other possible switching mechanism? On the other hand, it is still far from clear on the characteristics of the switching processes due to various switching mechanisms. In this work, we focus on recognizing the hidden switching mechanisms and presenting the detailed characteristics of the switching processes by performing three-dimensional (3D) phase-field simulations. Particularly, the effects of depolarization, shear strain and flexoelectricity on the mechanical switching of epitaxial BTO nanofilms are separated out (figure 1). The films are supposed to be under ideal surface screening and the mechanical switching behaviors in both normal and sliding loading modes are simulated. We show that the depolarization field due to the polarization inhomogeneity induced by the tip loads can lead to bidirectional mechanical switching. The coupling between shear strain and polarization is also verified to be one of possible sources of mechanical switching. The role of flexoelectricity on the mechanical switching is revisited, and a great impact of flexoelectricity-modified polarization boundary condition is found. At last, attention is paid to the influencing factors of the mechanical switching process, including loading force, misfit strain, temperature and film thickness, etc, with the volume of the switched domain in function of these factors being given. The unique characteristics of each switching mechanism are emphasized and should be useful for the experimental verification of the potential mechanisms. The revealed tunability of the switching by various factors is also instructive for the design and optimization of related ferroelectric devices based on mechanical engineering.

2. Model and methodology

2.1. Mechanical modeling of the tip-film contact

In this work, our model systems are (0 0 1) BTO nanofilms subjected to PFM tip-force. The films are supposed to be epitaxially grown on substrates with a compressive in-plane misfit strain, such as $La_{0.67}Sr_{0.33}MnO_3$ (LSMO). The PFM tip-force

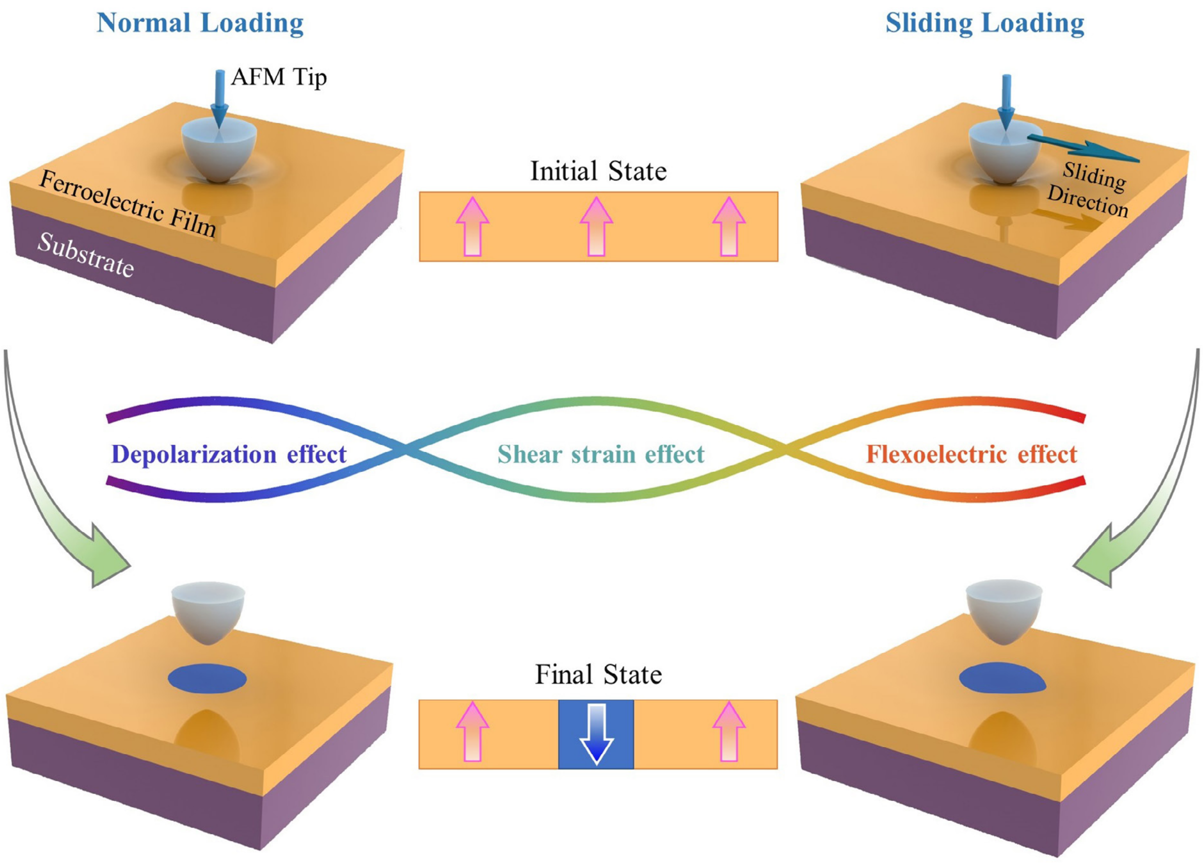

Figure 1. Schematic of the tip-induced mechanical switching in ferroelectric thin films for both normal loading mode and sliding loading mode. The switching process involves the crossover of depolarization effect, shear strain effect and flexoelectric effect.

generates an inhomogeneous deformation in the films, and consequently causes the redistribution of polarizations. For different PFM loading modes, i.e. the normal loading mode and the sliding loading mode, the PFM tip results in different strain fields, which will lead to distinct responses of dipoles and polarization switching behaviors.

In the following, the tip-film systems are placed in a Cartesian coordinate system denoted as (O, x_1, x_2, x_3). To obtain the polarization switching behaviors under the two loading modes, the tip-film contact problems need be solved at first to obtain the proper distributions of the stress and strain fields. In previous works [20, 25], the strain field in the film under the normal loading mode is calculated by applying the analytical stress distribution of Hertz contact pressure on the top surface [27], i.e. $\tau_3 = -3p_{\text{load}}/(2\pi a^2)\sqrt{1 - r^2/a^2}$ for spherical tips, with r being the distance from the tip-surface junction, p_{load} the loading force, and a the radius of contact area. However, this method falls in trouble for the sliding loading mode due to the difficulties on the analytical solution of dynamic contact problem with friction. Therefore, finite element method (FEM) is employed here to numerically solve the tip-film contact problem and obtain the stress and strain distributions in the film caused by the tip loads, for both the normal and sliding loading modes.

It is a static contact problem for the normal loading mode. For the sliding loading mode, the tip possesses a velocity along the sliding direction x_1 to mimic the dynamic contact problem. For simplicity, in the FEM model, the PFM tip is assumed to be in spherical shape. Coulomb friction model is adopted to describe the tip-surface contact. In the Coulomb model, it is assumed that no relative motion occurs in the contact areas if the equivalent frictional stress, i.e. the tangential traction,

$$\tau_{\text{t}} = \sqrt{\sigma_{13}^2 + \sigma_{23}^2} \tag{1}$$

is smaller than a critical stress τ_{c}. Here, σ_{13} and σ_{23} are the shear stress components at the contact surface. The τ_{c} is proportional to the contact pressure σ_{33}, i.e.

$$\tau_{\text{c}} = \mu\sigma_{33} \tag{2}$$

where μ is the Coulomb friction coefficient. The slipping occurs when the equivalent frictional stress reaches the critical stress, i.e.

$$\tau_{\text{t}} = \tau_{\text{c}}. \tag{3}$$

2.2. Phase-field model with flexoelectricity

To capture the domain pattern evolution of ferroelectric nanofilms under tip loads, the phase-field model is employed in this work. The spontaneous polarization field $\mathbf{P}(\mathbf{r}, t) = (P_1, P_2, P_3)$ is chosen as the order parameter field [28]. In this model, the evolution of order parameter field $\mathbf{P}(\mathbf{r}, t)$ is described by the time-dependent Ginzburg–Landau (TDGL) equations,

$$\frac{\partial P_i(\mathbf{r},t)}{\partial t} = -M\frac{\delta F}{\delta P_i(\mathbf{r},t)} \tag{4}$$

where F is the total free energy of the system, M is the kinetic coefficient and t is time.

The Gibbs free energy is adopted as we consider a film subjected to external stress. Taking flexoelectricity into account, the total free energy of a ferroelectric film can be written as

$$F = \iiint [f_{\text{Land}} + f_{\text{elas}} + f_{\text{elec}} + f_{\text{grad}} + f_{\text{flexo}}]\mathrm{d}V + \iint f_{\text{surf}}\mathrm{d}S. \tag{5}$$

Where f_{Land}, f_{elas}, f_{elec}, f_{grad}, f_{surf} and f_{flexo} are the energy densities of bulk Landau energy, elastic energy, electrostatic energy, gradient energy, surface energy and flexoelectric coupling energy, respectively.

For BTO, the bulk Landau energy density can be written as a polynomial expansion up to eighth order and takes the form [29],

$$\begin{aligned} f_{\text{Land}}(P_i) = {} & a_1\sum_i P_i^2 + a_{11}\sum_i P_i^4 + a_{12}\sum_{i>j} P_i^2P_j^2 + a_{111} \\ & \sum_i P_i^6 + a_{112}\sum_{i\neq j} P_i^4P_j^2 + a_{123}\prod_i P_i^2 \\ & + a_{1111}\sum_i P_i^8 + a_{1112}\sum_{i\neq j} P_i^6P_j^2 + a_{1122} \\ & \sum_{i>j} P_i^4P_j^4 + a_{1123}\sum_{i\neq j\neq k, j>k} P_i^4P_j^2P_k^2 \end{aligned} \tag{6}$$

where a_i, a_{ij}, a_{ijk}, and a_{ijkl} are the Landau–Devonshire coefficients.

The elastic energy density can be written as

$$f_{\text{elas}}(P_i,\sigma_{ij}) = -\frac{1}{2}s_{ijkl}\sigma_{ij}\sigma_{kl} - Q_{ijkl}\sigma_{ij}P_kP_l \tag{7}$$

where s_{ijkl} is the compliance tensor of material, σ_{ij} is the stress tensor and Q_{ijkl} is the electrostrictive tensor. Hereafter in the paper, the Einstein summation convention is assumed (if not explicitly declared) for the repeated subscripts from 1 to 3.

For a material with spontaneous polarizations, based on the concept of background dielectric constant, the electrostatic energy density is given by

$$f_{\text{elec}}(P_i,E_i) = -P_iE_i - \frac{1}{2}\varepsilon_{\text{b}}E_iE_i \tag{8}$$

where $\varepsilon_{\text{b}} = \varepsilon_0 + \chi_{\text{b}}$ is the background dielectric constant with ε_0 and χ_{b} being the vacuum permittivity and background susceptibility respectively [30, 31], and E_i is the total electric field.

To consider the energy penalty caused by the polarization gradient, we include the following gradient energy density in the system's free energy,

$$f_{\text{grad}}(P_{i,j}) = \frac{1}{2}g_{ijkl}P_{i,j}P_{k,l} \tag{9}$$

where g_{ijkl} is gradient energy coefficient tensor. The comma in $P_{i,j}$ means the spatial differentiation of P_i with respect to the jth coordinate.

The surface energy density describes the intrinsic effect of polarization variation in out-of-plane direction because of the truncation at the surface of the film, and it can be simply written as

$$f_{\text{surf}}(P_i) = \frac{1}{2}\left(\frac{D_1^S}{\delta_1^{\text{eff}}}P_1^2 + \frac{D_2^S}{\delta_2^{\text{eff}}}P_2^2 + \frac{D_3^S}{\delta_3^{\text{eff}}}P_3^2\right) \tag{10}$$

where D_i^S are coefficients related to the surface orientations and the gradient energy coefficients, and δ_i^{eff} are extrapolation lengths [32].

Flexoelectric effect denotes the coupling between polarization and strain gradient, and is phenomenologically written as [33],

$$P_i = \mu_{ijkl}\varepsilon_{jk,l}. \tag{11}$$

Here μ_{ijkl} is the flexoelectric tensor and $\varepsilon_{jk,l}$ is the strain gradient. The strain tensor is given by $\varepsilon_{jk} = \frac{1}{2}(u_{j,k} + u_{k,j})$, with u_i being the displacement. In the total free energy, the flexoelectric effect is reflected by the flexoelectric coupling energy [18, 19],

$$f_{\text{flexo}}(P_i,\varepsilon_{ij,l}) = -\frac{f_{ijkl}}{2}(P_k\varepsilon_{ij,l} - \varepsilon_{ij}P_{k,l}) \tag{12}$$

where f_{ijkl} is the flexoelectric coupling coefficients.

The dynamics of a ferroelectric is a process with co-evolution of the polarization field, mechanical field and electric field. We thus also need to calculate the mechanical field and electric field. As the mechanical field and electric field generally have much smaller relaxation times than that of the polarization field, we can solve the two fields according to the corresponding equilibrium equations. Note that the consideration of flexoelectricity modifies the electromechanical constitutive equations and contributes additional terms in the mechanical equilibrium equation and the boundary condition. The modified stress–strain relations can be written as

$$\sigma_{ij} = c_{ijkl}(\varepsilon_{kl} - \varepsilon_{kl}^0) + f_{ijkl}P_{k,l} \tag{13}$$

where c_{ijkl} is the elastic coefficient tensor and $\varepsilon_{kl}^0 = Q_{ijkl}P_kP_l$ is the eigenstrain due to electrostriction. Thus, the mechanical equilibrium equation takes the form

$$\sigma_{ij,j} = c_{ijkl}(\varepsilon_{kl,j} - \varepsilon_{kl,j}^0) + f_{ijkl}P_{k,lj} = 0. \tag{14}$$

Assuming that there are no other charges in the film except the polarization charges, the electrostatic equilibrium equation is given by

$$D_{i,i} = 0 \tag{15}$$

where $D_i = \varepsilon_{\text{b}}E_i + P_i$ is the electric displacement.

At the top and bottom surfaces of the film, the polarization boundary condition is given by letting the variation of the total free energy with respect to polarization to zero. It takes the form [34, 35],

$$\left(\frac{D_i^S}{\delta_i^{\text{eff}}}P_i + n_jg_{ijkl}P_{k,l} + n_j\frac{f_{lmij}}{2}\varepsilon_{lm}\right)\Big|_{h_0,h_f} = 0 \tag{16}$$

where n_j are the direction cosines of the surfaces, h_0 and h_f denote the positions of the bottom and top surfaces of the film, respectively.

The stress boundary condition at the top surface of the film can be written as

$$\sigma_{ij}n_j|_{h_f} = \tau_i \tag{17}$$

where τ_i are the surface traction components resulting from the PFM tip loads.

Moreover, for a film with the ideal short-circuit condition, the electrical boundary condition at the top surface and bottom interface of the film is given by

$$\varphi|_{h_0,h_f} = 0 \tag{18}$$

where φ is the electric potential.

Suppose that the in-plane dimensions of the film are infinite. Periodic polarization conditions are employed for all the fields in the in-plane directions (x_1 and x_2 directions).

2.3. Numerical implements

In the FEM model, the PFM tip is spherical with a radius of 50 nm. The tip material is chosen as Pt, which is commonly used in the experiments. The Young's modulus and Poison's ratio of Pt are 158 GPa and 0.35, respectively. For BTO, its elastic stiffness coefficients are $c_{11} = 275$ GPa, $c_{12} = 179$ GPa, and $c_{44} = 54$ GPa [36]. The elastic stiffness coefficients of the substrate are taken to be those of LSMO, i.e. $c_{11} = 180$ GPa, $c_{12} = 100$ GPa, and $c_{44} = 56$ GPa [37]. The thickness of the substrate is set to be three times as that of BTO film, which balances the accuracy in calculating the strain/stress field of the film and the calculation efficiency. The bottom surface of the substrate is encastred. Quadratic Lagrange interpolation shape function is used to solve the contact problems and extract the surface traction τ_i. The contact pressure and tangential force are calculated by the augmented Lagrangian method [38]. The friction coefficient μ is set to be 0.3, according to the previous works [16, 17, 39, 40]. In the normal loading mode, the tip indents with a series of indentation depths by applying the displacement boundary condition on the top surface of the tip. The tip load, i.e. the reacting force, is then calculated by integrating the stress components over the whole top surface of the film. Various indentation cases are calculated to obtain the tip load and the corresponding stress and strain distributions. The applied tip load in this study varies from 200 nN to 2000 nN. Hexagonal meshes are employed for the film and substrate, and the mesh size in vicinity of the tip-film contact area is about 0.8 nm. Tetragonal meshes are employed for the spherical tip, and the mesh size is about 0.4 nm near the contact area.

In the phase-field simulations, the parameters of the free energy densities are taken to the same with previous work [41]. The TDGL equation (equation (4)) under the polarization boundary condition (equation (16)) is solved by finite difference method on a regular mesh grid $128 \times 128 \times N$ with the grid spacing being 0.4 nm. The total thickness of the film is thus $0.4 \times N$ nm. The reduced time step is set to be $\Delta t^* = 0.01$ in unit of $|Ma_1|_{300\,\mathrm{K}}$. The mechanical and electrostatic equilibrium equations (equations (14) and (15)) are solved on the same mesh grid by the fast Fourier transform technique (FFT) which is based on the Khachaturyan's microscopic elastic theory and the Stroh's formalism of anisotropic elasticity [42]. In addition, a 'two-step scheme' is used to obtain the elastic field [25]. In this scheme, the stress boundary condition (equation (17)) is also adopted at the bottom interface of the film when solving the polarization evolution, where the surface tractions of the bottom interface are retrieved from the stress fields of the film/substrate system given by the FEM calculation.

In the FFT method, the strain field satisfying the mechanical equilibrium equation (equation (14)) under stress boundary condition (equation (17)) is divided into the homogeneous part and inhomogeneous part. The homogeneous part can be readily determined via the mechanical equilibrium equation. The inhomogeneous part is solved as follows. First, equation (14) is solved under the periodic boundary condition in all of the three directions and the solution is denoted as $u_i^A(\mathbf{r})$. In the 3D Fourier space, the solution is,

$$v_k^A(\mathbf{g}) = -\mathrm{i}g^2\Omega_{ik}^{-1}(\mathbf{m})g_j\sigma_{ij}^*(\mathbf{g}) \tag{19}$$

where $\mathbf{g}$ is the reciprocal lattice vector with g being its length and g_j being its jth component, $\mathbf{m} = \mathbf{g}/g$ is the unit reciprocal lattice vector, and

$$v_k^A(\mathbf{g}) = \int_{-\infty}^{\infty}\int_{-\infty}^{\infty}\int_{-\infty}^{\infty} u_k^A(\mathbf{r})\mathrm{e}^{-\mathrm{i}\mathbf{g}\cdot\mathbf{r}}\mathrm{d}^3r \tag{20}$$

$$\sigma_{ij}^*(\mathbf{g}) = \int_{-\infty}^{\infty}\int_{-\infty}^{\infty}\int_{-\infty}^{\infty} [c_{ijkl}\varepsilon_{kl}^0(\mathbf{r}) - f_{ijkl}P_{k,l}(\mathbf{r})]\mathrm{e}^{-\mathrm{i}\mathbf{g}\cdot\mathbf{r}}\mathrm{d}^3r \tag{21}$$

$$g^2\Omega_{ik}^{-1}(\mathbf{m}) = G_{ik}^{-1}(\mathbf{g}) = c_{ijkl}g_jg_l = g^2c_{ijkl}m_jm_l \tag{22}$$

with m_i being the component of $\mathbf{m}$. Thus, the displacement in real space $u_i^A(\mathbf{r})$ can be obtained by the inverse Fourier transformation,

$$u_i^A(\mathbf{r}) = \frac{1}{(2\pi)^3}\int_{-\infty}^{\infty}\int_{-\infty}^{\infty}\int_{-\infty}^{\infty} v_i^A(\mathbf{g})\mathrm{e}^{-\mathrm{i}\mathbf{g}\cdot\mathbf{r}}\mathrm{d}^3g. \tag{23}$$

Second, the solution, denoted as $u_i^B(\mathbf{r})$, should be found to satisfy the equation,

$$c_{ijkl}u_{k,lj}^B(\mathbf{r}) = 0 \tag{24}$$

and fulfill the periodic boundary condition along the in-plane directions (x_1 and x_2) as well as the following boundary condition at the top and bottom surfaces of the film,

$$c_{i3kl}u_{kl}^B|_{h_0,h_f} = [c_{i3kl}(\varepsilon_{kl}^0 - u_{k,l}^A) - f_{i3kl}P_{k,l} + \frac{f_{i33l}}{2}P_{l,3} - \frac{f_{ij3l}}{2}P_{l,j}]|_{h_0,h_f}. \tag{25}$$

In the in-plane 2D Fourier space, by using

$$v_k^B(g_1, g_2, x_3) = \int_{-\infty}^{\infty}\int_{-\infty}^{\infty} u_k^B(x_1, x_2, x_3)\mathrm{e}^{-\mathrm{i}(g_1x_1+g_2x_2)}\mathrm{d}^3r. \tag{26}$$

Equation (24) changes to be

$$c_{i\alpha k\beta}(\mathrm{i}g_\alpha)(\mathrm{i}g_\beta)v_k^B + (c_{i\alpha k3} + c_{i3k\alpha})(\mathrm{i}g_\alpha)v_{k,3}^B + c_{i3k3}v_{k,33}^B = 0 \quad \alpha, \beta \sim 1, 2. \tag{27}$$

The general solution of equation (27) is,

$$v_k^B(g_1, g_2, x_1) = a_k \mathrm{e}^{\mathrm{i}px_3\sqrt{g_1^2+g_2^2}} \tag{28}$$

where a_k and p are coefficients determined by the boundary condition (equation (25)). The displacement in real space $u_i^B(\mathbf{r})$ is given by the 2D inverse Fourier transformation,

$$u_i^B(\mathbf{r}) = \frac{1}{(2\pi)^3}\int_{-\infty}^{\infty}\int_{-\infty}^{\infty} v_i^B(g_1, g_2, x_3)\mathrm{e}^{-\mathrm{i}(g_1x_1+g_2x_2)}\mathrm{d}g_1 dg_2. \tag{29}$$

Then the total inhomogeneous strain can be obtained by adding $u_i^A(\mathbf{r})$ and $u_i^B(\mathbf{r})$.

Using the similar scheme, one can obtain the electric field by solving equation (15) under the boundary condition equation (18). To validate the solutions of FFT method, calculation based on FEM on hexagonal meshes is also conducted to solve the electrostatic equation. The depolarization fields calculated by FFT and FEM methods in a film with random polarization configuration, uniform polarization configuration $P_1 = 0,\ P_2 = 0,\ P_3 = x_3/h$ and nonuniform polarization configuration $P_1 = \sin(x_1),\ P_2 = \sin(x_2),\ P_3 = \sin(x_3)$ are shown in supplementary figure S1 (stacks.iop.org/JPhysCM/31/145701/mmedia). It can be seen that the results of two methods agree very well.

3. Results and discussion

The phase-field method enables us to separate out the roles of specific effects in the mechanical switching process by turning on/off the corresponding energy contributions in the free energy, which brings us a good route to explore the mechanisms of mechanical switching. A typical phase-field simulation of the mechanical switching process consists of the following three steps. At first, the film is initialized into a single-domain state with an upward or downward polarization and is sufficiently relaxed to reach the steady state. Secondly, the tip force is applied (load-on) to the film and the polarization field of the film is relaxed to reach a new steady state. Finally, the tip force is removed (load-off) and the polarization field of the film evolves to a final state, which is compared with the initial state to see whether switching occurs.

Considering the difference in strain distributions between the normal and sliding loading modes, as depicted in figure 2, the switching behaviors of the film under the two loading modes are both simulated to make a comparison. In fact, from figure 2, we can see that the strain distributions are of high symmetry with respect to the tip-film contact axis for the normal loading mode, while the symmetry is broken for the sliding loading mode. Take the distributions of ε_{11} and ε_{13} as examples. For the sliding loading mode, ε_{11} is negative (compressive) near the leading edge along the tip motion, and is positive (tensile) near the trailing edge; meanwhile, ε_{13} has a large positive value in the area beneath the tip. These asymmetric profiles are distinguishable with those of the normal loading mode, which are either symmetric or antisymmetric with respect to the tip-film contact axis.

3.1. Separating the roles of depolarization, shear strain and flexoelectric effect in mechanical switching

In the very beginning of the study, we first simulate the domain evolution of a film under tip loads when none of the depolarization effect (denoted as 'E'), shear strain effect (denoted as 'Q_{44}'), and flexoelectric effect (denoted as 'F') is considered. This can give us a first insight into the influences of the other effects on the mechanical switching process and provide a contrast simulation for further analysis of the roles of 'E', 'Q_{44}' and 'F'. It is shown that no polarization is switched when none of these three effects considered, indicating that the other effects could not induce mechanical switching (see supplementary figure S2).

Then we start to reveal separately the role of 'E', 'Q_{44}', and 'F' in the mechanical switching process of BTO films. When one of the three effects is considered, the other two effects is excluded by turning off the corresponding energy terms in the total free energy. The mesh grid is set to be $128 \times 128 \times 12$, which corresponds to a 4.8 nm thick film. The compressive misfit strain is set to be -0.020 and the room temperature (300 K) is adopted. The film is initialized to a single-domain state with an upward polarization. The normal tip force is 1500 nN. Figures 3(a) and (b) depict the 3D plots of the steady domain patterns at the load-on and load-off steps for the normal loading mode (denoted as 'Press') and sliding loading mode (denoted as 'Slide'), respectively, when only 'E' is considered. The polarization configuration in vicinity of the tip-surface contact area is zoomed on to more clearly see the domain pattern morphology. The domain orientations assigned with different colors are defined as follows: '$a+$' domain when $|\mathbf{P}| > 0.1$ (in unit of $P_0 = 0.26$ C m^{-2}), $P_1 > 0$ and $|P_1|/|\mathbf{P}| > 0.8$; '$a-$' domain when $|\mathbf{P}| > 0.1$, $P_1 < 0$ and $|P_1|/|\mathbf{P}| > 0.8$; '$b+$' domain when $|\mathbf{P}| > 0.1$, $P_2 > 0$ and $|P_2|/|\mathbf{P}| > 0.8$; '$b-$' domain when $|\mathbf{P}| > 0.1$, $P_2 < 0$ and $|P_2|/|\mathbf{P}| > 0.8$; '$c+$' domain when $|\mathbf{P}| > 0.1$, $P_3 > 0$ and $|P_3|/|\mathbf{P}| > 0.8$; '$c-$' domain when $|\mathbf{P}| > 0.1$, $P_3 < 0$ and $|P_3|/|\mathbf{P}| > 0.8$. The remaining parts of the domain pattern are denoted as 'other'.

From figure 3(a), one can see that under the consideration of 'E', the polarization at the edge of the tip-surface contact area flips to downward direction when the tip force is load-on for the normal loading mode. Meanwhile, the polarization in the region surrounded by the ring of flipped polarization has a small magnitude $|\mathbf{P}| < 0.1$, thus the domain state of this region is denoted as 'other'. The polarization distribution is always symmetric with respect to the tip axis due to the symmetry of the tip load profile. When the tip force is removed, the polarization field finally evolves to a cylindrical 180° domain pattern. While the domain pattern is rather different for the sliding loading mode. As depicted in figure 3(b), the polarization switching occurs mainly at the leading edge along the tip sliding direction, rather than at the surrounding edge of the

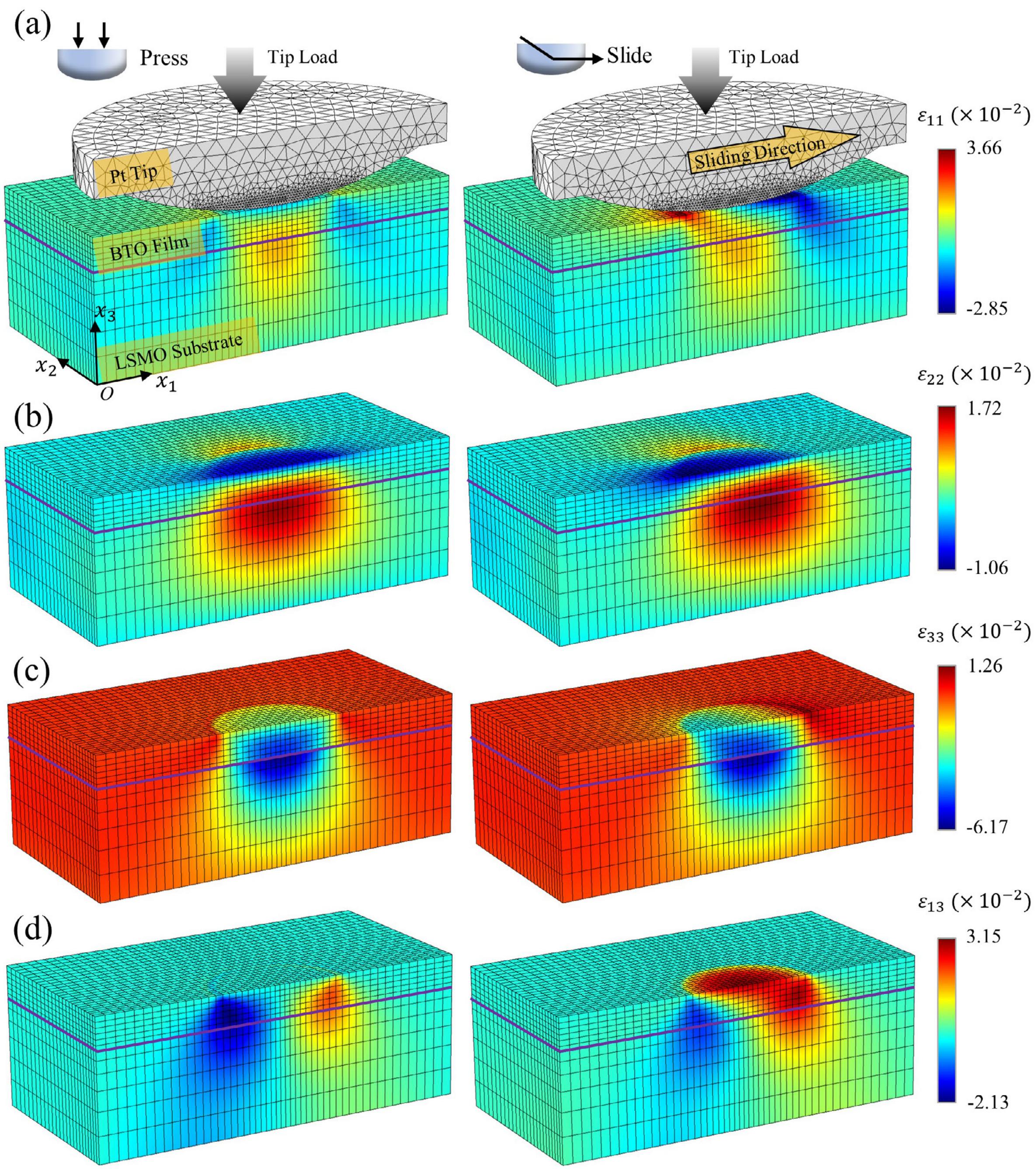

Figure 2. The strain field of $BaTiO_3/La_{0.67}Sr_{0.33}MnO_3$ system induced by a spherical Pt tip (in radius of 50 nm) under a load force of 1500 nN for both normal and sliding loading mode, calculated by FEM. 'Press' denotes the normal loading mode and 'Slide' denotes the sliding loading mode. (a)–(d) Correspond to the distributions of strain ε_{11}, ε_{22}, ε_{33} and ε_{13}, respectively.

contact area for the normal loading mode. The dipole configuration is obviously not symmetric with respect to the tip center, due to the asymmetry of strain distributions induced by the sliding tip. After the polarization relaxation at the load-off step, a crescent '$c-$' domain forms at the leading edge along the tip motion. Generally, the domain patterns during the switching process demonstrate that 'E' is one of the switching mechanisms in mechanical switching.

The effect of coupling between shear strain and polarization ('Q_{44}') on the mechanical switching behavior is reflected by the energy term $-\frac{1}{2}Q_{44}(\sigma_{12}P_1P_2+\sigma_{13}P_1P_3+\sigma_{23}P_2P_3)$ in the total free energy. With consideration of only 'Q_{44}', the domain patterns in the switching process is depicted in figures 3(c) and (d) for the normal and sliding loading mode, respectively. It can be seen from figure 3(c) that, for the normal loading mode, the region beneath the tip with a small polarization magnitude (denoted as 'other' domain) is similar with the contrast simulation without 'E', 'Q_{44}' and 'F' (supplementary figure S2). During the whole loading process, no mechanical switching occurs. When the tip force is removed, the film recovers to the initial '$c+$' domain state. However, for the sliding loading mode, the case is quite different. From figure 3(d), it can be seen that the tip affected region of the film exhibits a complex domain pattern when the tip force is

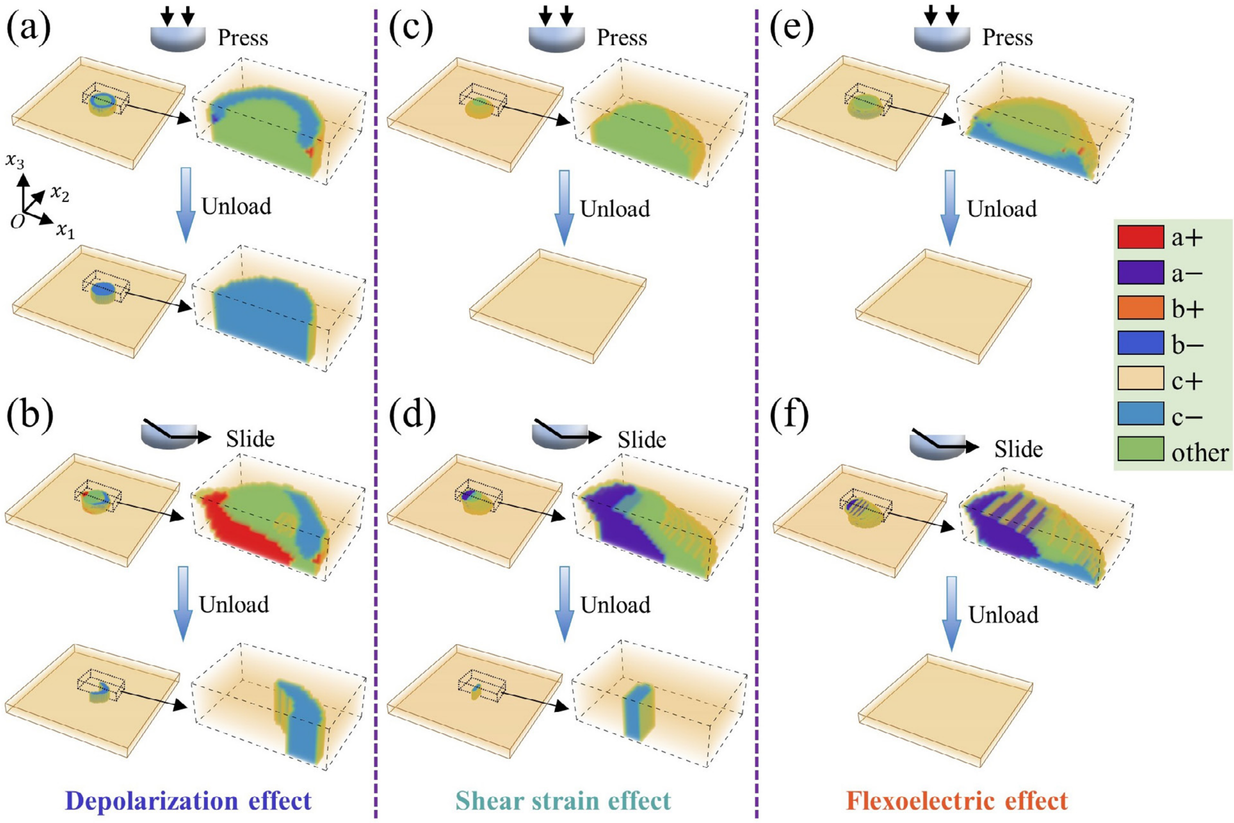

Figure 3. Tip-force induced domain patterns of a film with respective consideration of depolarization effect (‘E’), shear strain effect (‘Q_{44}’) and flexoelectric effect (‘F’). (a) and (b) depict the steady domain patterns under the effect of ‘E’ when the tip is loaded on or off for normal loading mode and sliding loading mode, respectively. (c) and (d) depict the steady domain patterns under the effect of ‘Q_{44}’ when the tip is loaded on or off for normal loading mode and sliding loading mode, respectively. (e) and (f) depict the steady domain patterns under the effect of ‘F’ when the tip is loaded on or off for normal loading mode and sliding loading mode, respectively.

exerted. At the trailing edge along the tip sliding direction, the tip force results in the ‘$a-$’ domain pointing opposite to the sliding direction. Meanwhile, at the region just beneath the tip center, the ‘other’ domain is produced. Between these two kinds of domains is the mechanically switched ‘$c-$’ domain in the upper part of the film. After the polarization relaxation at the load-off step, a thin tabular ‘$c-$’ domain is found. Thus, it is implied that the ‘Q_{44}’ is also one of the switching mechanisms in mechanical switching under sliding loading force.

Moreover, flexoelectricity is believed to be an important effect responsible for the observed mechanical switching of ferroelectric polarization in experiment. However, the effect of flexoelectricity alone on mechanical switching without the consideration of ‘E’ and ‘Q_{44}’ has not been reported, as well as the effect of polarization boundary condition modified by flexoelectricity (equation (16)). Here we also conduct a separate consideration of the flexoelectric effect in the mechanical switching process for both the normal and sliding loading modes, with turning on/off the flexoelectricity-modified polarization boundary condition. In the total free energy, the flexoelectric coupling energy term is included, whereas the energy terms related to ‘E’ and ‘Q_{44}’ are excluded. The flexoelectric coupling coefficients are set to be $f_{11} = 3.072$ V, $f_{12} = 1.992$ V and $f_{44} = 0.027$ V [20, 43].

The effect of the flexoelectricity-modified polarization boundary condition is first inspected. The 3D plots of the steady domain patterns at the load-on and load-off steps for the normal and sliding loading modes are depicted in figures 3(e) and (f), respectively. It can be seen that for the normal loading mode, the domain orientation at the upper part of the film beneath the tip is still ‘$c+$’ when the tip force is loaded on; however, the domain orientation at the lower part of the film is switched to be ‘$c-$’. When the tip force is removed, the film recovers to its initial ‘$c+$’ domain due to the existence of ‘$c+$’ domain at the upper part of the film. For the sliding loading mode, ‘$a-$’ domain pointing opposite to the sliding direction is generated at the trailing edge of tip motion. At the upper part of the film near the leading edge, ‘$c+$’ domain remains stable. Meanwhile, at the lower part of the film near the leading edge, ‘$c-$’ domain is induced. After loading off, the film also recovers to the initial ‘$c+$’ single domain state due to the ‘$c+$’ domain at the upper part of the film. Therefore, it is demonstrated that flexoelectric effect can actually lead to polarization switching when the tip-force is load-on. While it may be confusing that the switched ‘$c-$’ domain recovers to the initial ‘$c+$’ single domain when the tip-force is load-off because of the ‘$c+$’ domain at the upper part of the film. In fact, the existence of ‘$c+$’ domain at the upper part of film is a result of the flexoelectricity-modified

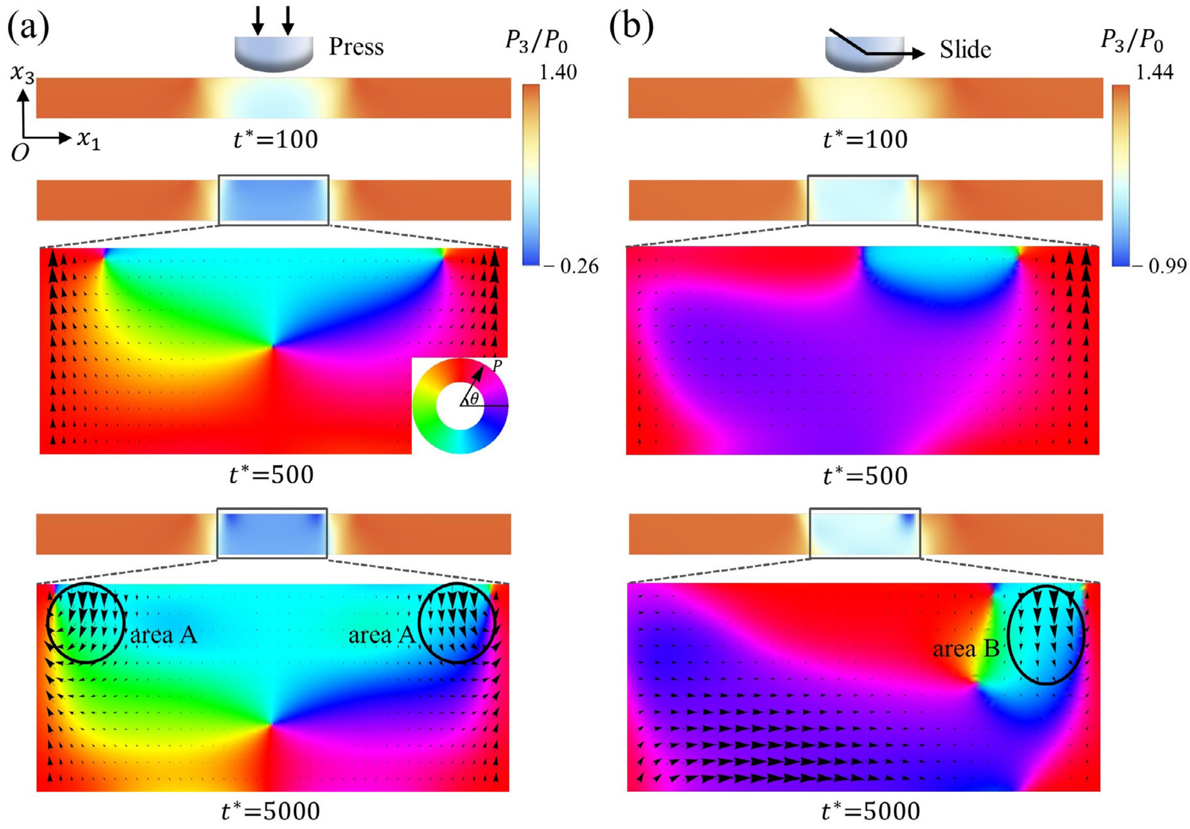

Figure 4. Analysis of mechanical switching induced by '*E*'. (a) and (b) are the snapshots of polarization evolution in the middle x_1Ox_3 plane ($x_2 = L_2/2$) at the load-on step for normal loading mode and sliding loading mode, respectively.

polarization boundary condition. It is reasonable that the effect of the polarization boundary condition is so obvious, considering that only '*F*' is considered here while '*E*' and 'Q_{44}' not. Actually, a detailed explanation for this confusing phenomenon will be given in section 3.4.

3.2. Switching process and mechanism of depolarization effect ('E')

To understand how the depolarization effect '*E*' induces polarization switching, the polarization evolution snapshots during the switching process is helpful. Figures 4(a) and (b) depict the snapshots of polarization evolution at the load-on step for the normal and sliding loading modes, respectively, with the slice view at the middle x_1Ox_3 plane ($x_2 = L_2/2$) being presented. Here L_2 denotes the length of the simulation box in x_2 direction. The dipole configuration beneath the tip at the time step $t^* = 500$ and $t^* = 5000$ is also amplified with the color indicating the polarization direction. For the normal loading mode, from figure 4(a), one can see that the polarization evolution is along the following path: the polarization under the tip first exhibits a sharp decrease, whereas the polarization is still upward (see the polarization component P_3 at time step $t^* = 100$); then the polarization of the upper region of film under the tip gradually flips to downward, with a small polarization magnitude ($t^* = 500$); further, the switched area gradually expands and the magnitude of the flipped polarization near the edge of tip-surface contact area (see 'area A' as marked in the figure) increases to be as large as $P_3^* = -0.26$ ($t^* = 5000$). While for the sliding loading mode, the switching process is very different. As depicted in figure 4(b), the overall polarization at the region beneath the tip also undergoes a sharp decrease when the tip force is loaded on ($t^* = 100$). Then polarization switching occurs subsequently at the leading edge along the tip sliding direction ($t^* = 500$), rather than at the surrounding edge of the contact area for the normal loading mode. Later on, the switched region shifts a small distance along the sliding direction and the magnitude of the flipped polarization increases to be $P_3^* = -0.99$ ('area B' as marked in the figure), with the polarization at the bottom of film under the tip pointing along the tip sliding direction ($t^* = 5000$).

The switching mechanism due to the depolarization effect, as well as the difference in the switching characteristics between the normal and sliding loading modes, can be inferred from the evolution of the depolarization field (see supplementary figure S3). In fact, though the film is under perfect surface screening, the mechanical tip load can still induce a large depolarization field, which is due to the large polarization inhomogeneity under the tip load. It should be noted that the increase of the magnitude of flipped polarization in the marked areas 'area A' and 'area B' in figure 4 is mainly caused by the mechanical strain rather than the depolarization field. This can be inferred by comparing the polarization field

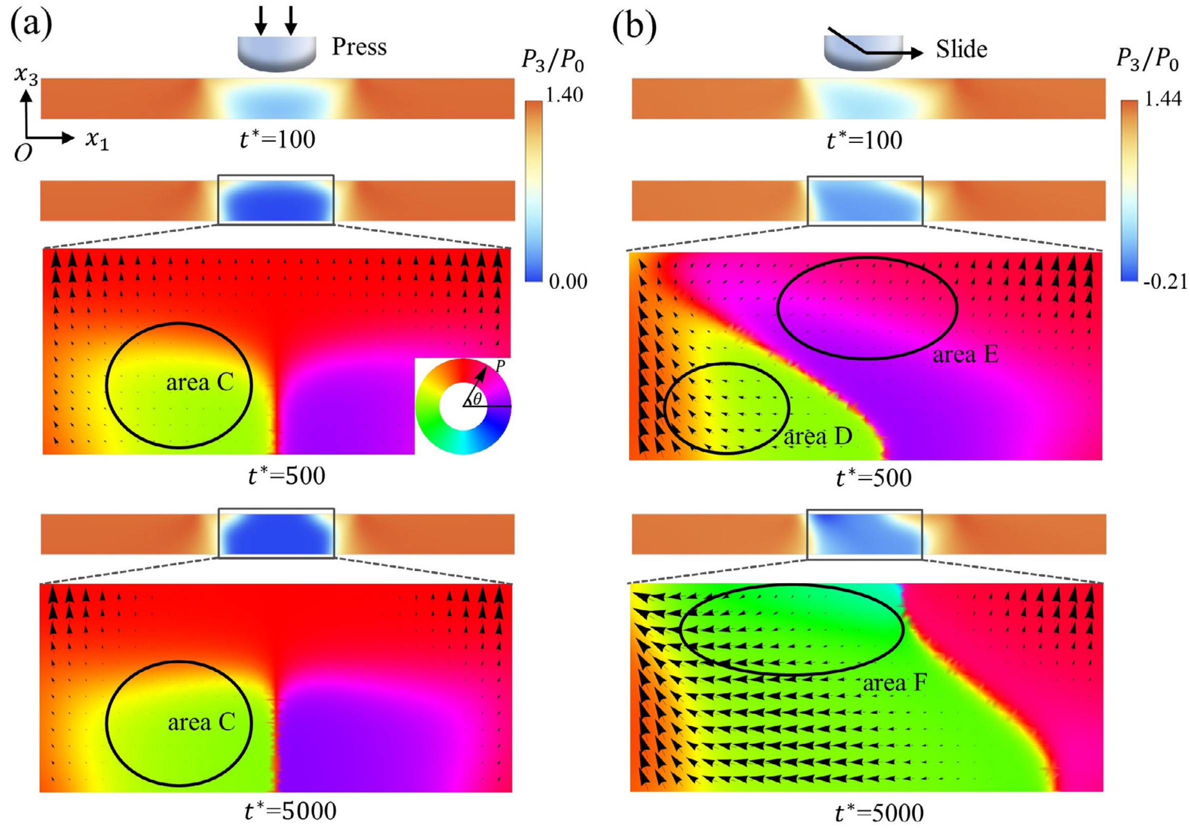

Figure 5. Switching process and mechanism in the presence of coupling between shear strain and polarization ('Q_{44}'). (a) and (b) are the snapshots of polarization evolution in the middle x_1Ox_3 plane ($x_2 = L_2/2$) at the load-on step for normal loading mode and sliding loading mode, respectively.

there with that in the same area in supplementary figure S2. This indicates that the depolarization field plays an important role during the stage of domain nucleation rather than domain growth. Note also that the negative depolarization field is large in the top region of the film beneath the tip for the normal loading mode, whereas it possesses a large negative value only near the leading edge for the sliding loading mode. Due to such different distribution features of the depolarization field, the switched regions and the resultant domain patterns of the two loading modes are quite different.

3.3. Switching process and mechanism of shear strain effect ('Q_{44}')

To obtain the switching process and mechanism of the shear strain effect in mechanical switching, the polarization evolution snapshots of the middle x_1Ox_3 plane at the load-on step when 'Q_{44}' is considered are shown in figures 5(a) and (b) for normal and sliding loading mode, respectively. It can be seen that for the normal loading mode, the consideration of 'Q_{44}' introduces polarization rotation especially in the bottom part of the film, e.g. in the 'area C' and its symmetric part with respect to the tip center in figure 5(a), compared with supplementary figure S2. From time $t^* = 100$ to $t^* = 5000$, the polarization magnitude gradually decreases and the polarization continues to reorient. The polarization distribution at the bottom part of the film is also symmetric due to the symmetry of the normal loading force. The polarization component P_3 is always positive during the whole loading process. For the sliding loading mode, the switching process also experiences a polarization rotation and a decrease of the polarization magnitude. At $t^* = 500$, a tilted domain wall forms to separate the region possessing positive P_3 and negative P_1 ('area D') with the region possessing positive P_3 and positive P_1 ('area E'). Then, 'area D' gradually expands and merges with a part of 'area E', pushing the domain wall to shift along the tip sliding direction. It is noteworthy that near the top surface of the film, the positive P_3 of the expanded 'area D' is switched to be negative at $t^* = 5000$. This results in the marked region 'area F' possessing negative P_3 and negative P_1.

In fact, the energy term related to the mechanical switching occurring at the x_1Ox_3 plane is mainly '$-c_{44}Q_{44}\varepsilon_{13}P_1P_3$', in the form of shear strain. In this formula, we have $c_{44} > 0$ and $Q_{44} > 0$. Therefore, to reach an energy minimum, a positive sign of the product $\varepsilon_{13}P_1P_3$ is favored. That is, if $\varepsilon_{13} > 0$, P_1 and P_3 tend to be all positive or all negative; whereas if $\varepsilon_{13} < 0$, P_1 and P_3 tend to have opposite signs. The distributions of ε_{13} at the middle x_1Ox_3 plane ($x_2 = L_2/2$) for the two loading modes are depicted in supplementary figures S4(a) and (b), respectively. It can be seen that for the normal loading mode, ε_{13} is antisymmetrically distributed with respect to the tip axis, with $\varepsilon_{13} > 0$ at the right part of tip and $\varepsilon_{13} < 0$ at the left part of tip. The shear strain just beneath the tip is quite small compared with that at the surrounding regions. Such

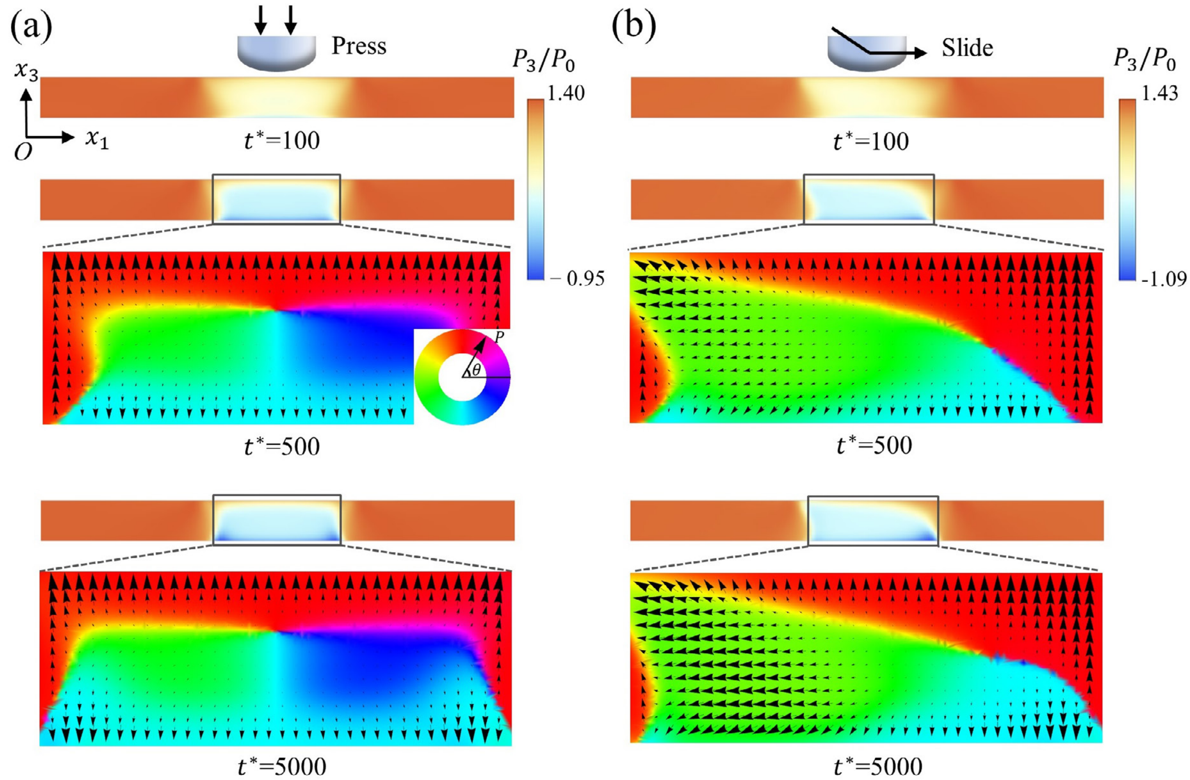

Figure 6. Analysis of mechanical switching induced by 'F'. (a) and (b) are the snapshots of polarization evolution in the middle x_1Ox_3 plane ($x_2 = L_2/2$) at the load-on step for normal loading mode and sliding loading mode, respectively.

an antisymmetric distribution of the shear strain results in the symmetric polarization distribution as shown in figure 5(a). Specifically, the 'area C' possessing positive P_3 and negative P_1 corresponds to the $\varepsilon_{13} < 0$ region at the left part of the tip. This polarization orientation satisfies the energy minimum related to the 'Q_{44}' term. While the distribution of ε_{13} for the sliding loading mode is more complex (see supplementary figure S4(b)) than that of the normal loading mode. Though ε_{13} is also negative and positive at the left and right part of tip, respectively, a significant difference is the $\varepsilon_{13} > 0$ region just beneath the tip. We consider that it is the positive shear strain of this region that induces the mechanical switching behavior. In this region, the positive P_3 of the expanded 'area D' is driven to have the same sign with the negative P_1, leading to the appearance of 'area F' with downward P_3 to guarantee the energy minimum.

For the sliding loading mode, the key of the polarization switching is the expansion of 'area D' by occupying the region 'area E' just beneath the tip. It is noteworthy that the energy minimum of the 'Q_{44}'-related energy is satisfied at both 'area D' and 'area E', because of their opposite signs in ε_{13} and P_1. So one concerning issue is why the 'area D' occupies 'area E' rather than vice versa or remaining unchanged. We speculate that the driven force is still the elastic energy, which can further be verified by the evolution of energy curves in section 3.5. As a matter of fact, the expansion of 'area D' can be illustrated by the distribution of ε_{11} just beneath the tip for the sliding loading mode in figure 2(a). Right beneath the tip, ε_{11} is relatively tensile at the bottom of the film compared with that near the top surface of the film. Thus, the area possessing in-plane polarization P_1 at the bottom of the film should be larger than that near the top surface, due to the mechanical compatibility by electrostriction. From figure 5(b), we find that the major part of 'area D' is at the bottom, whereas the major part of 'area E' is near the top surface. For both 'area D' and 'area E', the major part possesses a larger area with in-plane polarization P_1. Therefore, the expansion of 'area D' is favored due to its larger area possessing P_1 at the bottom of the film than that near the top surface, which further assists the polarization switching by the coupling between shear strain and polarization.

3.4. Switching process and mechanism of flexoelectric effect ('F')

When 'F' is considered, the snapshots of the polarization evolution of the middle x_1Ox_3 plane when the tip force is exerted are shown in figures 6(a) and (b) for the two loading modes, respectively. It can be seen from figure 6(a) that for the normal loading mode, the magnitude of polarizations beneath the tip also experiences a sharp decrease, when the tip-force is load-on, e.g. at $t^* = 100$. Afterwards, the polarizations at the lower part of film are switched downward and the magnitude of polarizations gradually increase and lead to the domain pattern in figure 3(e). It is noteworthy that the magnitude of downward polarizations at the bottom interface is larger than that at the other regions of the film. Also, the magnitude of upward polarization at the top surface of the film is larger than that of other regions with upward polarization. For the sliding loading mode, the evolution of polarizations is similar. The major difference is the large in-plane polarizations pointing opposite to the sliding direction at the trailing edge of tip motion. In fact, the P_3 component of these in-plane polarizations is positive near the film surface, but it is negative near the bottom interface. To better illustrate the polarization switching induced by 'F', distributions of the flexoelectric field at different time steps are depicted in supplementary figures S5(a) and (b) for the normal and sliding loading modes, respectively. One can see that for the normal loading mode, the flexoelectric field is negative (i.e. downward) beneath the tip. The value of the negative flexoelectric field is approximately -2×10^7 V m^{-1}. For the sliding loading mode, the magnitude of the negative flexoelectric field is a little larger, with a maximum at the trailing edge along the tip sliding direction. This also coincides with the reported studies [16, 17]. It is the negative flexoelectric field that drives the polarizations to switch to be downward.

Though the polarization switching occurs driven by the flexoelectric field at the load-on step, the existence of the upward polarizations at the upper part of the film for both of two loading modes is abnormal, considering the large negative flexoelectric field at the top surface of the film. These abnormal upward polarizations are also shown in figures 3(e) and (f) as the confusing '$c+$' domain at the upper part of film. Understanding the formation of this abnormal '$c+$' domain is important as the '$c+$' domain influences the stability of the switched '$c-$' domain significantly and leads to the recovery of the initial '$c+$' domain when the tip force is removed. Actually, the enhanced magnitude of polarization P_3 at the film surface and interface implies that the polarization boundary condition may play a significant role in this abnormal behavior. At the top surface and bottom interface, the polarization boundary condition related to P_3 is modified by the flexoelectric effect as,

$$\frac{\partial P_3}{\partial z}|_{h_f,h_0} = \mp\frac{P_3}{\delta_3^{\mathrm{eff}}} - \frac{1}{2G_{11}}[f_{12}(\varepsilon_{11}+\varepsilon_{22})+f_{11}\varepsilon_{33}]. \tag{30}$$

Under the compressive in-plane misfit strain and tip load, the flexoelectricity-relevant term, i.e. $-\frac{1}{2G_{11}}[f_{12}(\varepsilon_{11}+\varepsilon_{22})+f_{11}\varepsilon_{33}]$, leads to the polarization boundary condition $\partial P_3/\partial z > 0$ both at the top surface and bottom interface. This partial differential means that a larger positive P_3 at the top surface and a larger negative P_3 at the bottom interface are preferred, which is the case in figures 6(a) and (b). We therefore speculate that this flexoelectricity-modified polarization boundary condition is the reason of the existence of an abnormal '$c+$' domain at the upper part of the film beneath the tip and suppresses the mechanical switching.

To further elaborate this point, we conduct another simulation by employing the polarization boundary condition without the flexoelectricity-relevant term and the result is shown in supplementary figure S6. Actually, the whole domain beneath the tip is switched downward for the two loading modes when the flexoelectricity-relevant term in the polarization boundary condition is removed, with no '$c+$' being induced. Therefore, it shows that the flexoelectricity-relevant term in the polarization boundary condition indeed has a great effect on the mechanical switching behaviors. This term tends to prevent the polarization switching under the conditions in this study. Furthermore, though it seems strange that no '$c-$' domain is obtained after the loading-off step when the flexoelectricity-modified polarization boundary condition is considered as depicted in figures 3(e) and (f), it is still reasonable since here only the flexoelectricity is considered. Once the effect of depolarization 'E' is included, the large positive P_3 component at the top surface of the film is not favored due to the large depolarization field, which will make the impact of the flexoelectricity-modified polarization boundary condition not apparent and lead to successful switching. In other words, our result indicates that the depolarization effect may plays an important role in the mechanical switching caused by flexoelectricity.

3.5. Switching mechanisms from the perspective of free energy

To get a deeper understanding of the switching mechanisms mentioned above, the evolution curves of different free energies at the load-on step are shown in figure 7 for all of the three switching mechanisms, with both of the two loading modes being considered. figures 7(a) and (b) depict the free energy evolutions under the effect of 'E' for normal and sliding loading modes, respectively. It can be seen that the main contribution of the decrease of total free energy is the reduction of elastic energy, which is a typical feature of mechanical switching. At the beginning of the evolution, e.g. $t^* < 100$, the elastic energy exhibits a sharp decrease to meet the mechanical compatibility, via reducing the magnitude of polarization below the tip. The polarization reduction is responsible for the decrease of the Landau energy. On the contrary, the electrostatic energy increases in this stage, which is caused by the local polarization inhomogeneity due to polarization accommodation under the tip load. Afterwards ($t^* > 100$), the electrostatic energy gradually decreases, corresponding to the process of downward polarization nucleation to avoid an otherwise large depolarization field. Meanwhile, as a result of the gradual growth of the flipped polarization, the elastic energy continues to decrease and the Landau energy gradually increases. One can note that the trends in the energy evolution curves for the two loading modes are similar, due to their identical polarization switching mechanism.

Figures 7(c) and (d) depict the evolution curves of the energy term related to 'Q_{44}' when the tip-force is loaded on for normal and sliding loading modes, respectively, with the insets presenting the evolution curves of the other energy terms. It shows that, for the normal loading mode, the 'Q_{44}'-related energy decreases rapidly in the beginning ($t^* < 300$), which corresponds to the polarization reorientation in the film. Afterwards, the 'Q_{44}'-related energy curve climbs up a little bit and approaches to a stable level. The increase of the 'Q_{44}'-related energy here can be explained by the decrease of the magnitude of polarization. Take 'area C' in figure 5 as an example, the typical polarization value $P_1^* = -0.01$ and $P_3^* = 0.17$ at $t^* = 300$ decreases to $P_1^* = -0.001$ and $P_3^* = 0.04$ at $t^* = 5000$. The energy term

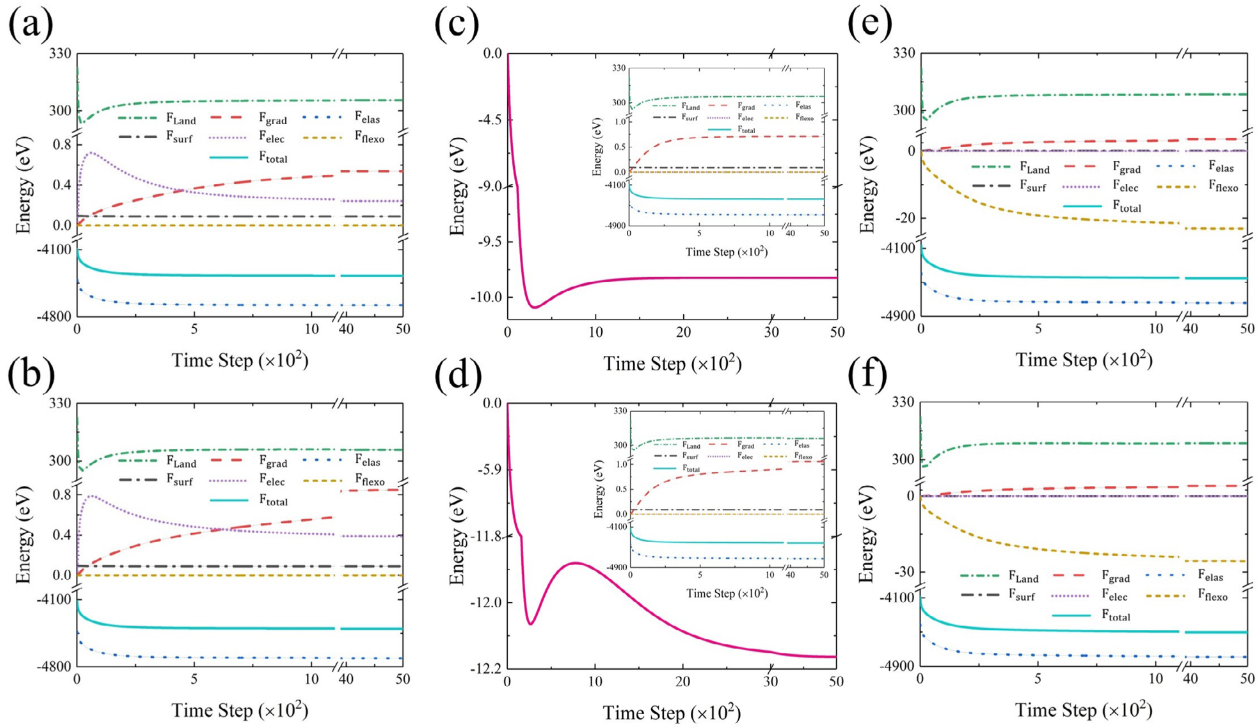

Figure 7. Evolution curves of free energies when different switching mechanisms are considered. (a) and (b) depict the evolution curves of the free energy terms when 'E' is considered for normal loading mode and sliding loading mode, respectively. (c) and (d) depict the evolution curves of the 'Q_{44}'-related energy when 'Q_{44}' is considered for normal loading mode and sliding loading mode, respectively, with the insets showing the evolution of other free energies. (e) and (f) depict the evolution curves of the free energy terms when 'F' is considered for normal loading mode and sliding loading mode, respectively.

'$-c_{44}Q_{44}\varepsilon_{13}P_1P_3$' is negative in this area, so the decrease of magnitude of P_1 and P_3 increases the 'Q_{44}'-related energy. The energy curve for the sliding loading mode also experiences the same sharp decrease in the beginning ($t^* < 300$) and the following climbing-up, but the curve exhibits an additional drop after about $t^* = 800$. The first sharp decrease also stems from the polarization rotation, while the reason of the climbing-up is different with that in the normal loading mode, because the polarization magnitude in 'area D' does not decrease in the following steps. This climbing-up is attributed to the expansion of the 'area D' by occupying the region 'area E' just beneath the tip. The 'area D' possesses positive P_3 and negative P_1, but the shear strain ε_{13} is positive beneath the tip, which leads to a positive energy term '$-c_{44}Q_{44}\varepsilon_{13}P_1P_3$' in this region and increases the energy. The P_3 beneath the tip is then driven by this positive energy contribution of this region to switch to be downward to reach the energy minimum, as is reflected by the additional drop of the curve.

For mechanical switching under the effect of 'F', the energy evolution curves during the switching process are shown in figures 7(e) and (f) for the two loading modes, respectively. It can be seen that the flexoelectric coupling energy exhibits a sharp decrease for both loading modes, indicating a deterministic role of flexoelectricity in the polarization switching.

3.6. Phase diagrams for different switching cases

So far we have shown that the depolarization field ('E') and the shear strain ('Q_{44}') can also induce mechanical switching, and have revisited the effect of flexoelectricity on the mechanical switching behavior. Nevertheless, the dependence of mechanical switching dominated by these mechanisms on various influencing factors is still not clear. This should be an important issue in terms of applications. On the one hand, a reveal of such dependence can provide us clues to identify the exact mechanisms that cause the mechanical switching in experiment. On the other hand, it can also instruct us how to achieve efficient mechanical switching. Therefore, we conduct a series of simulations to see the dependence of mechanical switching dominated by 'E', 'Q_{44}', 'F' or their combinations, e.g. '$E + F$', '$E + Q_{44}$' and '$E + F + Q_{44}$', on the circumstantial conditions by varying the influencing factors such as misfit strain, film thickness, temperature and tip force. The contrast simulations without considering the effects of 'E', 'Q_{44}' and 'F' (denoted as '*None*') are also performed to seek if there exist hidden mechanisms under a wide spectrum of conditions. The results are shown in supplementary figures S7–S12. To be short, there exists no other switching mechanism in a wide spectrum of physical conditions, besides 'E', 'Q_{44}' and 'F'. The switched volume induced by these switching mechanisms generally increases with the increase of temperature and force, and decreases with the increase of film thickness and compressive misfit strain, except for some anomalies for 'E', 'Q_{44}' and '$E + Q_{44}$'. The detailed tendencies of these curves and the corresponding explanations are given in supplementary material.

After revealing the roles of different mechanisms in the mechanical switching and their characteristics in a wide range

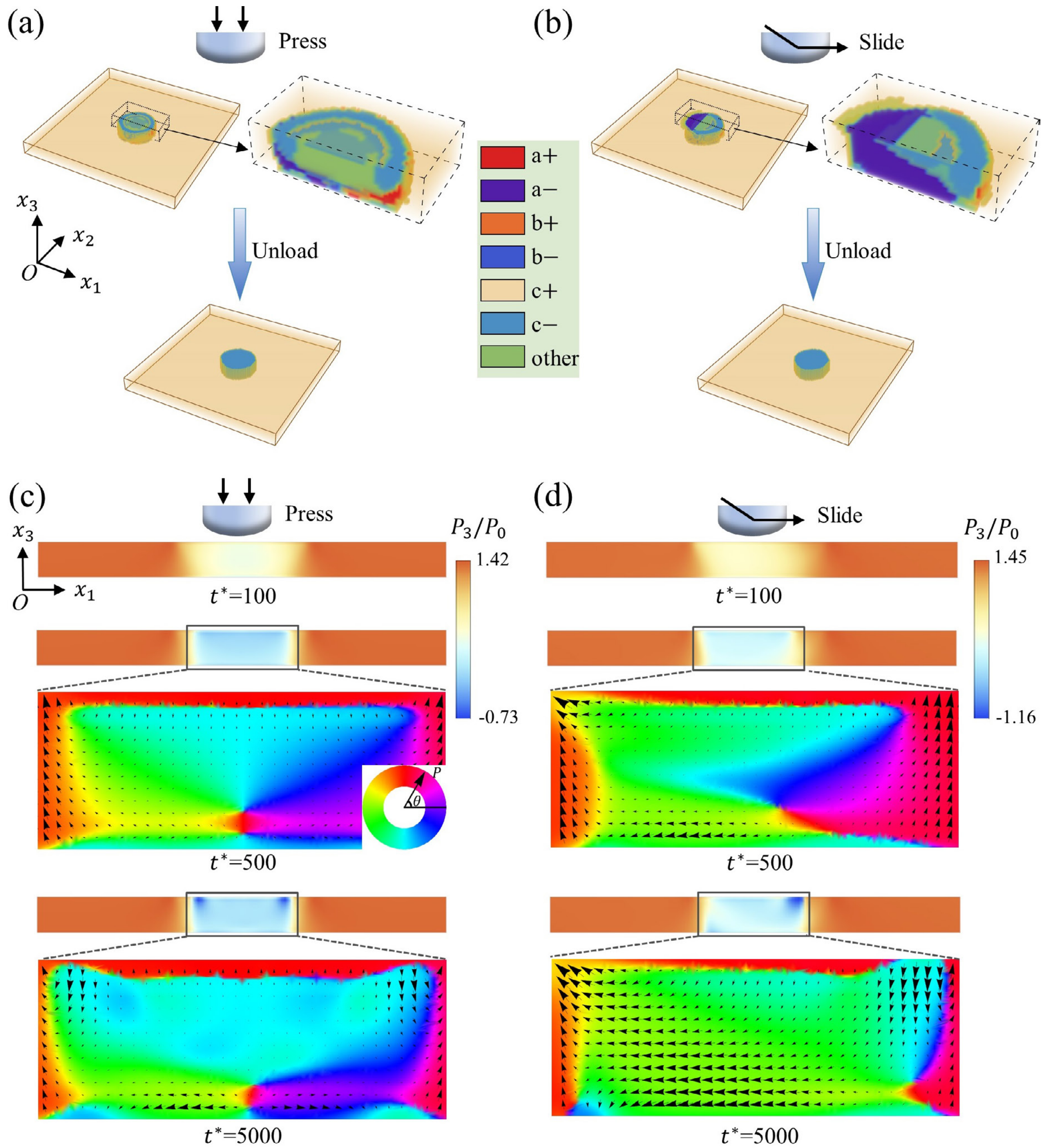

Figure 8. Tip-force induced domain evolution of a film in the presence of all of the three mechanisms, i.e. '$E + F + Q_{44}$'. (a) and (b) depict the steady domain patterns when the tip is loaded on or off for normal loading mode and sliding loading mode, respectively. (c) and (d) are the snapshots of polarization evolution in the middle x_1Ox_3 plane ($x_2 = L_2/2$) at the load-on step for normal loading mode and sliding loading mode, respectively.

of conditions, it is of practical significance to give an overall insight into the mechanical switching in films and obtain the phase diagrams of switched volume under the combining effects of the proposed mechanisms, i.e. '$E + F + Q_{44}$'. The domain patterns and switching process of '$E + F + Q_{44}$' are depicted in figure 8 for the two loading modes. Compared with the switching process under respective consideration of one single effect mentioned above, it can be seen that for the normal loading mode, the depolarization effect induces the large switched polarizations at the edge of the tip-surface contact area, and the flexoelectric effect leads to the polarization switching at the middle and lower part of the film. At upper part of film, the polarizations are switched by both 'E' and 'F'. It should be noted that the flexoelectric-modified polarization boundary condition also results in the relatively large upward polarization at the top surface and downward polarization at the bottom interface, while this effect is obviously depressed with the consideration of 'E' and 'Q_{44}' and has little influence on the stability of switched polarization. For the sliding loading mode, the depolarization effect induces the polarization switching at the leading edge of tip motion. The flexoelectric effect flips the polarizations at the trailing edge of tip

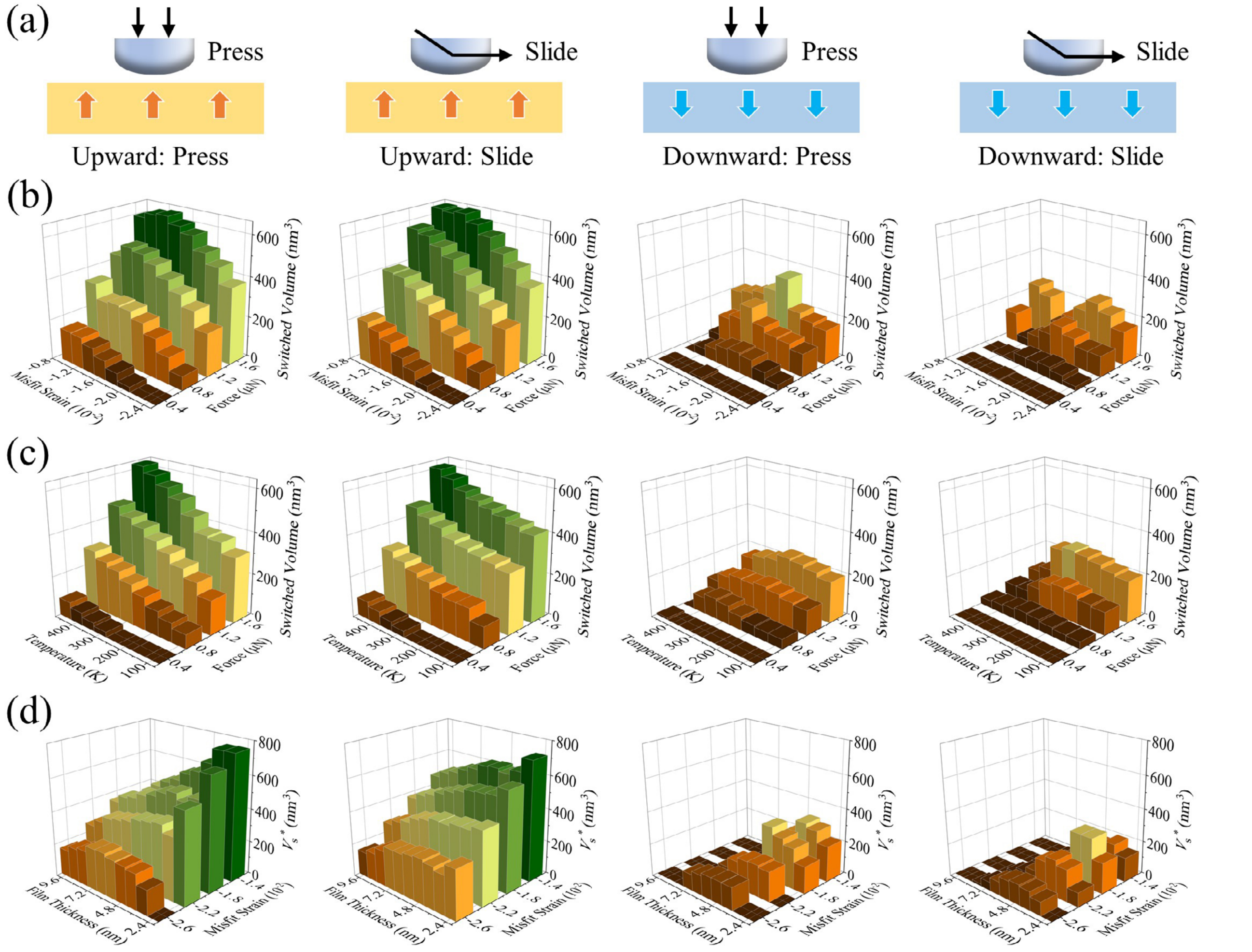

Figure 9. Phase diagrams of mechanical switching in films with both the initial upward and downward polarization, under the combining effects of the proposed mechanisms, i.e. '$E+F+Q_{44}$'. (a) Schematics of the four considered cases, (i) 'Upward: Press', (ii) 'Upward: Slide', (iii) 'Downward: press' and (iv) 'Downward: Slide'. (b) The misfit-strain versus tip-force phase diagram, (c) the temperature versus tip-force phase diagram, and (d) the film-thickness versus misfit-strain phase diagram, with panels from left to right corresponding to the four cases in (a).

motion. The polarizations just beneath the tip are switched under the combining effect of 'E', 'F' and 'Q_{44}'. It is noteworthy that for both of the normal and sliding loading modes, the polarizations decrease sharply when the tip-force is load-on. And there exist the near-paraelectric 'other' type domains which possess polarizations with small magnitude value at the steady state. Therefore, it is obvious that the switching processes experience an intermediate paraelectric phase, which has been speculated in [16] but not proved there.

To obtain the phase diagrams of switched volume under '$E+F+Q_{44}$', we focus on the following four switching cases: (i) switching in films with an initial '$c+$' single-domain state in normal loading mode (denoted as 'Upward: Press'), (ii) switching in films with an initial '$c+$' single-domain state in sliding loading mode ('Upward: Slide'), (iii) switching in films with an initial '$c-$' single-domain state in normal loading mode ('Downward: press'), and (iv) switching in films with an initial '$c-$' single-domain state in sliding loading mode ('Downward: Slide'). The schematics of the four cases are shown in figure 9(a). The switched volume of the four cases are calculated under a wide range of conditions (i.e. by varying the misfit-strain, tip-force, film-thickness and temperature). The misfit-strain versus tip-force phase diagram, the temperature versus tip-force phase diagram, and the film-thickness versus misfit-strain phase diagram are shown in figures 9(b)–(d), respectively, with panels from left to right corresponding to the four cases in figure 9(a). Particularly, the switched volume in figure 9(d) is normalized with respect to the film thickness $h_0 = 4.8\,\text{nm}$, i.e. $V_s^* = V_s h_0/h$, to get a better measure of the switching. From figure 9, it can be seen that for the cases with initial '$c+$' single-domain state, i.e. the cases 'Upward: Press' and 'Upward: Slide', the switched volume is generally much larger than that of cases with initial '$c-$' single-domain state. This stems from the flexoelectric effect since the tip force induced flexoelectric field is generally downward, which favors the 'up-to-down' polarization switching and prevents the 'down-to-up' polarization switching. The generally nonzero switched volume in the cases with initial '$c-$' single-domain state, i.e. the cases 'Downward: Press' and 'Downward: Slide', is due to the mechanisms 'E' and 'Q_{44}', which allow 'down-to-up' mechanical switching as their effects do not have a preferential

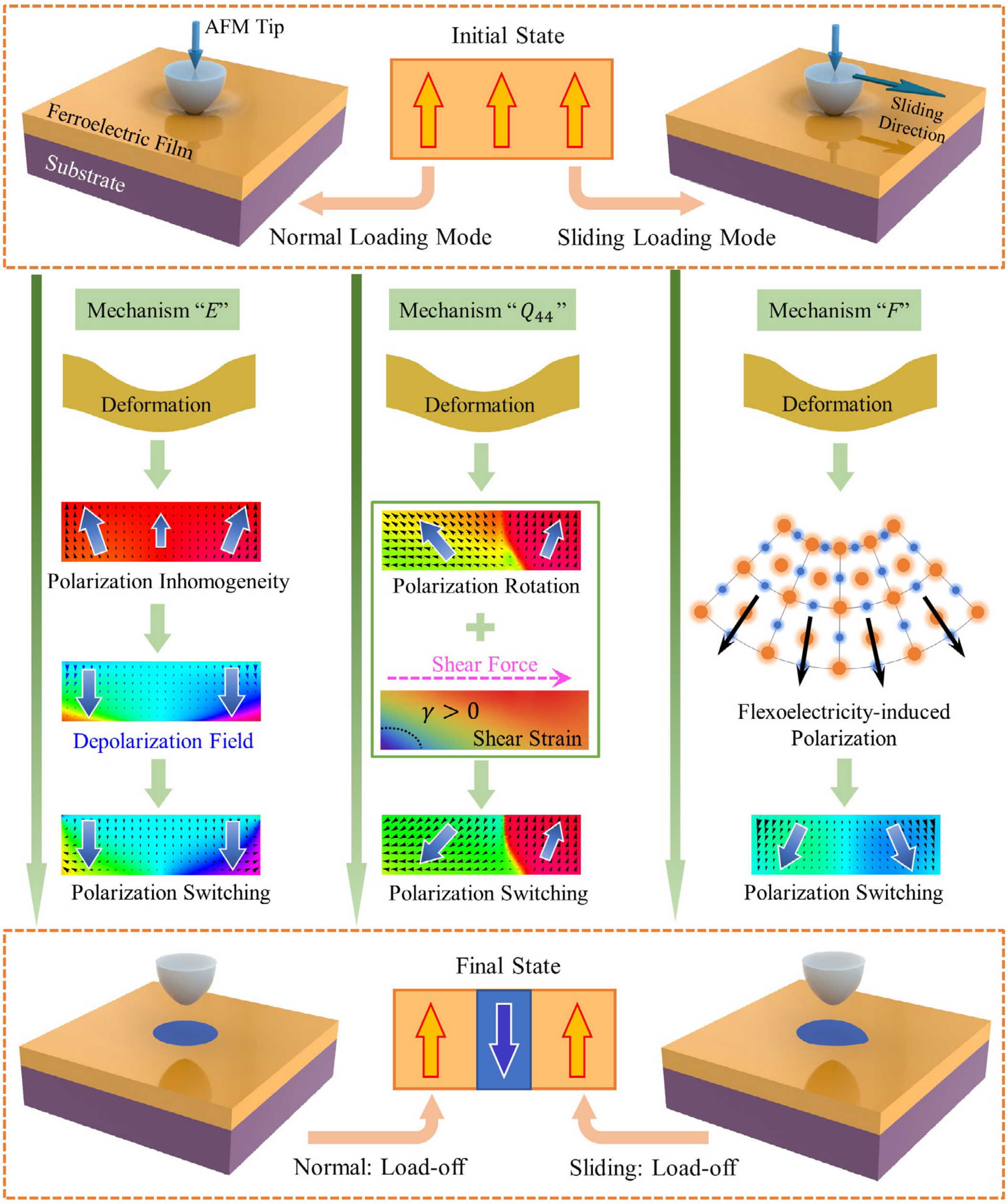

Figure 10. The summary schematic showing the three mechanisms of tip-induced mechanical switching in ferroelectric thin films for both normal loading mode and sliding loading mode.

direction and are equivalent for both initial upward and downward polarization. Moreover, for the cases with initial upward polarization, the switched volume generally increases with the increase of tip force and temperature, and decreases with the increase of film thickness and compressive misfit strain. An exception is found at compressive misfit strain (−0.026) for the normal loading mode, where the switched volume decreases at small film thickness region. Meanwhile, dependence of the switched volume on is much more complicated for the cases with initial downward polarization. Note, the switched volume of 'Upward: Slide' is generally larger than that of 'Upward: Press', i.e. the sliding loading mode can bring a more efficient switching than the normal loading mode, which is consistent with the trend observed in experiment [16]. Nevertheless, our result shows that the difference of the switched volume between the two loading modes is not obvious. This may be due to the difference of the sample conditions in our simulation and in experiment. Note, the uncertainty of the exact values of the flexoelectric coupling coefficients is probably another reason. For example, the shear coefficients used here is $f_{44} = 0.027$ V. A larger f_{44} would cause a more significant difference between the sliding and normal loading modes, considering the large shear strain gradient for the sliding loading mode.

4. Summary

In this work, we reveal the mechanical switching behaviors of BTO thin film under PFM tip force by performing a mass of 3D phase-field simulations. By turning on/off specific energy contributions, simulations are conducted to separately out the effects of depolarization field ('E'), the coupling between shear strain and polarization ('Q_{44}') and flexoelectricity ('F') on the mechanical switching behaviors. The results indicate that even though the film is under ideal surface screening condition, the depolarization field induced by the polarization inhomogeneity can still lead to polarization switching for both the normal and sliding loading modes. Furthermore, the specific distribution of shear strain for the sliding loading mode can also result in the polarization switching via the trilinear coupling between shear strain and polarization components. The role of flexoelectricity in mechanical switching is also reexamined. It is found that while the downward flexoelectric field can switch the polarization, the flexoelectricity-modified polarization boundary condition tends to frustrate the polarization switching when only 'F' is considered alone. This frustration effect is largely depressed in situations when 'E' and 'Q_{44}' are present. The switching characteristics of cases dominated by various mechanisms are analyzed and the intermediate transition to the paraelectric phase is proved. In the end, phase diagrams of mechanical switching in films with an initial upward or downward polarization under tip force in either normal or sliding loading modes are presented. The feasibility of 'down-to-up' switching induced by 'E' and 'Q_{44}' is clearly seen. The novel switching mechanisms of 'E' and 'Q_{44}' indicate the complicate mechanical switching behaviors in experimental samples and a crossover of various mechanisms. Note the experimental verification of the potential switching mechanisms beyond flexoelectricity remain exclusive. The analysis of the experimental observation is also challenged due to the lack of a good knowledge on the possible mechanical switching sources. Experimental verification of the three possible switching sources, i.e. 'E', 'F' and 'Q_{44}', can be based on their unique characteristics as revealed in this work (e.g. shape of switched domain, sensitivity to the tip loading mode, feasibility of bidirectional switching, tunability by factors like film thickness and misfit strain, etc). The analysis of the influencing factors in this work is also instructive for the design and optimization of devices exploiting mechanical switching of ferroelectric domains.

It should be noted that though the three mechanisms, namely 'E', 'Q_{44}' and 'F', work in very distinct ways, mechanical switching due to these mechanisms is in general attributed to the same origin, i.e. strain gradient (inhomogeneous deformation), as the summary schematic shown in figure 10. Actually, for mechanism 'E', the depolarization field is induced by the polarization inhomogeneity, while the polarization inhomogeneity is the outcome of the inhomogeneous distribution of strain. For mechanism 'Q_{44}', the switching involves the expansion of 'area D' (figure 6), which is induced by the inhomogeneous distribution of in-plane strain across the film thickness. For mechanism 'F', it is well-known that the flexoelectric field stems directly from the strain gradient. The acting pathways of the three mechanisms can be simply elucidated as follows. Mechanism 'E': inhomogeneous deformation → polarization inhomogeneity → depolarization field → polarization switching; Mechanism 'Q_{44}': inhomogeneous deformation → asymmetric polarization rotation → large trilinear coupling energy due to shear strain → polarization switching; Mechanism 'F': inhomogeneous deformation → flexoelectric field → polarization switching. All these strain-gradient-induced switching mechanisms pave the way toward strain gradient engineering of ferroelectrics, and can provide us better designs of new devices in applications. For example, in tip-film architectures, 'down-to-up' switching is precluded by flexoelectricity, but it can be induced by 'E' and 'Q_{44}', making it possible to realize the bidirectional switching via strain gradient. This should be important in developing non-volatile ferroelectric memories free of electrical writing. Overall, as the strain gradients have been proved to be able to switch the polarization, control the distribution of oxygen vacancies [44] and tune the dielectric permittivity of film [45], the strain gradient engineering can bring us more possibilities in designing material systems with desirable functionalities. In addition, better approaches dealing with the continuously varying load for the sliding loading mode need to be developed to gain more insights into the difference between the normal and sliding loading modes. The optimization of mechanical switching with consideration of other influencing factors such as the stiffness of substrate also appeals to further investigations.

Acknowledgments

This work was supported by the National Key Basic Research Program of China (No. 2015CB351905), NSFC (Nos. 11672339, 11602310), and the Guangzhou Science and Technology Project (No. 201707020002). Y Zheng also thanks the Special Program for Applied Research on Super Computation of the NSFC-Guangdong Joint fund (the second phase), Fok Ying Tung Foundation, Guangdong Natural Science Funds for Distinguished Young Scholar and China Scholarship Council for support.

ORCID iDs

W J Chen https://orcid.org/0000-0002-9276-7369

References

[1] Damjanovic D 1998 *Rep. Prog. Phys.* **61** 1267
[2] Junquera J and Ghosez P 2003 *Nature* **422** 506
[3] Ji W, Yao K and Liang Y C 2010 *Adv. Mater.* **22** 1763
[4] Guyonnet J, Gaponenko I, Gariglio S and Paruch P 2011 *Adv. Mater.* **23** 5377
[5] Setter N *et al* 2006 *J. Appl. Phys.* **100** 051606
[6] Catalan G, Seidel J, Ramesh R and Scott J F 2012 *Rev. Mod. Phys.* **84** 119
[7] Scott J F 2007 *Science* **315** 954
[8] Eng L M 1999 *Nanotechnology* **10** 405
[9] Wada S, Kakemoto H and Tsurumi T 2004 *Mater. Trans.* **45** 178

[10] Damodaran A R, Agar J C, Pandya S, Chen Z, Dedon L, Xu R, Apgar B, Saremi S and Martin L W 2016 *J. Phys.: Condens. Matter* **28** 263001

[11] Chen X, Tang X, Chen X Z, Chen Y L, Guo X, Ge H X and Shen Q D 2015 *Appl. Phys. Lett.* **106** 042903

[12] Bhaskar U K, Banerjee N, Abdollahi A, Solanas E, Rijnders G and Catalan G 2016 *Nanoscale* **8** 1293

[13] Lu H, Bark C W, De Los Ojos D E, Alcala J, Eom C B, Catalan G and Gruverman A 2012 *Science* **336** 59

[14] Wen Z, Qiu X, Li C, Zheng C, Ge X, Li A and Wu D 2014 *Appl. Phys. Lett.* **104** 042907

[15] Guo E J, Roth R, Das S and Dörr K 2014 *Appl. Phys. Lett.* **105** 012903

[16] Očenášek J, Lu H, Bark C W, Eom C B, Alcalá J, Catalán G and Gruverman A 2015 *Phys. Rev.* B **92** 035417

[17] Park S M, Wang B, Das S, Chae S C, Chung J S, Yoon J G, Chen L Q, Yang S M and Noh T W 2018 *Nat. Nanotechnol.* **13** 366

[18] Yudin P V and Tagantsev A K 2013 *Nanotechnology* **24** 432001

[19] Zubko P, Catalan G and Tagantsev A K 2013 *Annu. Rev. Mater. Res.* **43** 387

[20] Gu Y, Hong Z, Britson J and Chen L Q 2015 *Appl. Phys. Lett.* **106** 022904

[21] Jiang L, Tang J, Zhou Y, Yang Q, Zhang Y, Guo L and Zhong X 2015 *Comp. Mater. Sci.* **108** 309

[22] Cao Y, Morozovska A and Kalinin S V 2017 *Phys. Rev.* B **96** 184109

[23] Kalinin S V, Kim Y, Fong D D and Morozovska A N 2018 *Rep. Prog. Phys.* **81** 036502

[24] Yang S M *et al* 2017 *Nat. Phys.* **13** 812

[25] Chen W, Liu J, Ma L, Liu L, Jiang G L and Zheng Y 2018 *J. Mech. Phys. Solids* **111** 43

[26] Chen W J, Yuan S, Ma L L, Ji Y, Wang B and Zheng Y 2018 *RSC Adv.* **8** 4434

[27] Fischer-Cripps A C 2007 *Introduction to Contact Mechanics, Mechanical Engineering Series* 2nd edn (New York: Springer)

[28] Chen L Q 2002 *Annu. Rev. Mater. Res.* **32** 113

[29] Li Y L, Cross L E and Chen L Q 2005 *J. Appl. Phys.* **98** 064101

[30] Tagantsev A K 2008 *Ferroelectrics* **375** 19

[31] Zheng Y and Woo C H 2009 *Appl. Phys.* A **97** 617

[32] Kretschmer R and Binder K 1979 *Phys. Rev.* B **20** 1065

[33] Kogan S M 1964 *Sov. Phys. Solid. State* **5** 2069

[34] Eliseev E A, Morozovska A N, Glinchuk M D and Blinc R 2009 *Phys. Rev.* B **79** 165433

[35] Yurkov A S and Tagantsev A K 2016 *Appl. Phys. Lett.* **108** 022904

[36] Hlinka J and Marton P 2006 *Phys. Rev.* B **74** 104104

[37] Darling T W, Migliori A, Moshopoulou E G, Trugman S A, Neumeier J J, Sarrao J L, Bishop A R and Thompson J D 1998 *Phys. Rev.* B **57** 5093

[38] Simo J C and Laursen T A 1992 *Comput. Struct.* **42** 97

[39] Mata M and Alcala J 2004 *J. Mech. Phys. Solids* **52** 145

[40] Mo Y, Turner K T and Szlufarska I 2009 *Nature* **457** 1116

[41] Chen W, Zheng Y, Feng X and Wang B 2015 *J. Mech. Phys. Solids* **79** 108

[42] Li Y L, Hu S Y, Liu Z K and Chen L Q 2002 *Acta Mater.* **50** 395

[43] Ponomareva I, Tagantsev A K and Bellaiche L 2012 *Phys. Rev.* B **85** 104101

[44] Das S *et al* 2017 *Nat. Commun.* **8** 615

[45] Damodaran A R *et al* 2017 *Nat. Commun.* **8** 14961